Mesozoic 003 (2): 121–139
https://www.mapress.com/mz/

Review

ISSN 3021-1859 (print edition)
MESOZOIC
ISSN 3021-1867 (online edition)

https://doi.org/10.11646/mesozoic.3.2.1
http://zoobank.org/urn:lsid:zoobank.org:pub:BBE1E7FC-CEAE-4C5D-A76B-3A0CCB1FB2A9

Lithium isotope constraints on Permian–Triassic continental weathering and multi-proxy comparison

LUKANG TANG[1, 2] & HUA ZHANG[1, *]

[1]*State Key Laboratory of Palaeobiology and Stratigraphy, Nanjing Institute of Geology and Palaeontology, Chinese Academy of Sciences, Nanjing 210008, China*
[2]*University of Chinese Academy of Sciences, Beijing 100049, China*
lktang@nigpas.ac.cn; https://orcid.org/0009-0009-8065-1631
hzhang@nigpas.ac.cn; https://orcid.org/0000-0002-5871-8264
**Corresponding author*

Abstract

The Permian–Triassic transition (P–Tr, *ca*. 251.9 Ma) witnessed the most severe mass extinction of the Phanerozoic, triggered by intense volcanic activity and associated environmental catastrophes. Continental silicate weathering is central to understanding both the mechanisms of the extinction and the prolonged Early Triassic warmth, yet changes in its intensity and flux remain controversial. Lithium (Li) isotopes (δ^7Li), a promising tracer of silicate weathering, have increasingly been applied to the P–Tr transition. However, δ^7Li records from different sedimentary archives (marine carbonates, shales, cherts, and terrestrial clastic rocks) show stark discrepancies: some indicate rapid enhancement of chemical weathering, others invoke marine reverse weathering as the dominant control, and terrestrial evidence points to intensified physical erosion but suppressed chemical weathering. These contradictions arise because the marine δ^7Li signal integrates multiple processes—continental weathering input, reverse weathering, and changes in the size of the oceanic Li reservoir—that cannot be disentangled by a single proxy. This review synthesises δ^7Li records with the Chemical Index of Alteration (CIA), strontium (Sr) isotopes, osmium (Os) isotopes, and magnesium (Mg) isotopes across the P–Tr transition. We demonstrate a pronounced "intensity-flux decoupling" in continental weathering, where traditional weathering indices (CIA) and terrestrial δ^7Li indicate that chemical weathering intensity (measured as the chemical depletion fraction, W/D) did not increase globally and may have even decreased, while radiogenic Sr and Os isotopes record a sharp rise in the total terrigenous material flux. This paradox is reconciled with a regime of rapid physical erosion with limited chemical leaching, driven by vegetation collapse and a shortened hydrological cycle. Meanwhile, extreme Early Triassic marine δ^7Li anomalies are largely controlled by enhanced reverse weathering and a likely reduced marine Li reservoir. A multi-proxy deconvolution framework thus allows a three-dimensional separation of weathering intensity, flux, and internal oceanic processes, offering a unified way to resolve current controversies. Future priorities include quantitative calibration of archive effects, systematic mapping of spatial heterogeneity, and numerical modelling of the marine Li cycle to advance quantitative understanding of Earth system crises in deep time.

Keywords: Permian–Triassic boundary, lithium isotopes, continental weathering, reverse weathering, multi-proxy comparison, intensity-flux decoupling

Introduction

The Permian–Triassic transition (*ca*. 251.9 Ma) marks the most devastating biotic crisis of the Phanerozoic—the end-Permian mass extinction (EPME)—which eliminated ~81% of marine species and ~89% of terrestrial species (Fan *et al*., 2020; Viglietti *et al*., 2021; Dal Corso *et al*., 2022). Extensive geochronological and geochemical evidence points to the Siberian Traps Large Igneous Province (STLIP) and contemporaneous circum-Pangaean arc volcanism as the primary trigger (Veevers & Tewari, 1995; Zhang *et al*., 2013; Liao *et al*., 2016; Spalletti & Limarino, 2017; Zhang *et al*., 2021). Volcanic activity and associated thermal metamorphism of country rocks injected massive amounts of CO_2, CH_4, and SO_2 into the ocean-land-atmosphere system (Svensen *et al*., 2009; Dal Corso *et al*., 2022), triggering a chain of environmental catastrophes: rapid global warming, drastic carbon-cycle perturbations, ocean acidification, expansion of anoxic waters, and collapse of terrestrial ecosystems (Joachimski *et al*., 2012; Sun *et al*., 2012; Schneebeli-Hermann *et al*., 2013; Clarkson *et al*., 2016; Lau *et al*., 2016; Jurikova *et al*., 2020; Jiao *et al*., 2023).

During this destabilisation and subsequent reorganisation of Earth's surface system, continental

Submitted: 24 Apr. 2026; accepted by Z. Feng: 15 May 2026; published: 5 Jun. 2026

silicate weathering plays a central role, linking deep volcanic processes, atmospheric chemistry, land-surface evolution, and marine biogeochemical cycles. On the one hand, silicate weathering consumes atmospheric CO_2, representing the most important carbon sink on geological timescales and regulating the intensity and duration of greenhouse climates. On the other hand, the flux and chemical speciation of weathering products (dissolved ions, nutrients, and detrital material) delivered to the ocean directly influence marine primary productivity, anoxia, and the carbonate compensation depth (Walker *et al*., 1981; Mackenzie & Kump, 1995). Therefore, accurately constraining the intensity, rate, and spatial pattern of continental weathering across the P–Tr transition is essential not only for understanding the trigger and perpetuation of the extinction but also for explaining the prolonged extreme warmth of the Early Triassic.

Extensive studies have examined P–Tr continental weathering using a multi-proxy toolkit, including major-element weathering indices (*e.g*., CIA, CIW, WIP), radiogenic isotopes (*e.g*., Sr, Os, Nd), and non-traditional stable isotopes (*e.g*., Mg, Ca, Li) (Korte *et al*., 2003, 2006; Sedlacek *et al*., 2014; Georgiev *et al*., 2015, 2020; Dudás *et al*., 2017; Cao *et al*., 2019; Wang *et al*., 2019; Chen *et al*., 2020; Liu *et al*., 2020; Hu *et al*., 2021; Liu & Selby, 2021; Xu *et al*., 2023). However, because different proxies have distinct source sensitivities, response timescales, and susceptibilities to post-depositional alteration, they often yield apparently contradictory interpretations of weathering behaviour at the P–Tr transition. For instance, studies based on the Chemical Index of Alteration (CIA) mostly indicate that chemical leaching intensity in source areas did not increase significantly, or even decreased, during the P–Tr transition (Chen *et al*., 2022; Xu *et al*., 2023; Ye *et al*., 2024), whereas seawater strontium ($^{87}Sr/^{86}Sr$) and osmium ($^{187}Os/^{188}Os$) isotope records consistently point to a sharp rise in terrigenous input flux during the Early Triassic (Liu & Selby, 2021; Wang *et al*., 2021; Liu *et al*., 2023; Nsingi *et al*., 2025). This apparent "intensity-flux decoupling"—where the rate of chemical alteration and the total mass flux appear to diverge—remains a central unresolved paradox in current P–Tr paleoweathering research.

In this context, lithium isotopes (δ^7Li) have emerged as a powerful new weathering tracer due to their unique geochemical behaviour. First, Li primarily traces silicate weathering and is unaffected by carbonate dissolution (Dellinger *et al*., 2020; Pogge von Strandmann *et al*., 2021). Second, Li isotope fractionation is not affected by biological activity (Lemarchand *et al*., 2010; Pogge von Strandmann *et al*., 2022). Third, Li isotope fractionation is independent of redox conditions. Its fractionation mechanisms during weathering are well understood and have been quantitatively constrained in modern catchment studies (Dellinger *et al*., 2015; Pogge von Strandmann *et al*., 2022).

In recent years, δ^7Li has been used to reconstruct global and regional weathering histories across the P–Tr transition. An early study of marine carbonates from the Meishan section (South China) found that seawater δ^7Li near the P–Tr boundary was significantly lower than the modern value, interpreted as direct evidence of a dramatic increase in the flux of low-δ^7Li riverine input from rapid weathering of fresh basalts following the STLIP eruption (Sun *et al*., 2018). However, longer-term records have revealed a more complex picture: some studies argue that seawater δ^7Li declined continuously through the Lopingian and remained low in the Early Triassic, suggesting that enhanced marine reverse weathering (authigenic clay formation) was the dominant driver of the signal (Cao *et al*., 2022); other investigations using shales and cherts show relatively higher Early Triassic seawater δ^7Li, also attributed to reverse weathering but with a different mechanistic interpretation—preferential removal of light Li (Rauzi *et al*., 2024). More critically, recent direct evidence from terrestrial clastic rocks in southwestern China indicates that the extinction interval was characterised by intensified physical erosion but lower chemical weathering efficiency (Ye *et al*., 2024), in sharp contrast to the "global chemical weathering enhancement" hypothesis. Moreover, Taylor *et al*. (2026), based on a systematic comparison of δ^7Li across different archives, proposed that the Early Triassic marine Li reservoir may have shrunk dramatically, shortening the oceanic residence time of Li so that seawater δ^7Li was no longer globally homogeneous—a fundamental challenge to the conventional premise of using marine records to infer global weathering fluxes.

These divergences clearly indicate that the δ^7Li fluctuations across the P–Tr transition cannot be explained by a single process; they likely reflect a complex interplay of continental silicate weathering input, removal by marine authigenic clays, and the breakdown of spatial uniformity in the marine Li cycle. Interpreting δ^7Li records from a single section or archive in isolation can easily lead to partial or even misleading conclusions. Therefore, it is imperative to place Li isotopes within a systematic multi-proxy comparison framework—together with major-element weathering indices, Sr-Os isotopes, and Mg-Ca isotopes—for comprehensive deconvolution and integration.

Using Li isotopes as the central thread, this review first outlines the principles of Li-isotope tracing of weathering and the assumptions underlying deep-time reconstructions. It then details key findings and existing controversies from marine and terrestrial δ^7Li records across the P–Tr transition. On this basis, δ^7Li is systematically compared

with Chemical Index of Alteration (CIA), strontium (Sr) isotopes, osmium (Os) isotopes, and magnesium (Mg) isotopes to assess how these proxies differ and complement one another in revealing weathering intensity, flux, and spatiotemporal heterogeneity. Finally, we discuss possible causes of current controversies, including changes in the size of the marine Li reservoir, archive effects, and regional differences in weathering responses, and outline future research directions. This review aims to provide a more comprehensive perspective on weathering-climate-ocean coupling during the end-Permian Earth system upheaval and to serve as a methodological reference for multi-proxy integrated studies of critical deep-time transitions.

Results

Lithium isotopes in terrestrial processes

How does continental weathering affect riverine δ^7Li?

Lithium concentrations in upper-crustal silicate minerals (~5–100 ppm) are much higher than those in carbonate minerals (<5 ppm) (Dellinger *et al*., 2020; Pogge von Strandmann *et al*., 2021). Riverine Li records therefore mainly reflect silicate weathering processes. The dissolution of silicate minerals produces little Li isotope fractionation, whereas strong fractionation mainly occurs during the formation of secondary minerals (Hindshaw *et al*., 2019). During secondary mineral formation, ^{6}Li is preferentially incorporated into clay minerals, leaving the residual dissolved phase enriched in ^{7}Li. Thus, riverine δ^7Li mainly reflects the balance among primary mineral dissolution, secondary mineral formation, and water–rock interaction time (Vigier *et al*., 2008; Hindshaw *et al*., 2019).

On the basis of these fractionation characteristics, early studies simplified the weathering response of Li isotopes into a binary end-member model of "weathering-limited" (high δ^7Li) and "supply-limited" (low δ^7Li) regimes (Huh *et al*., 2001; Tomascak, 2004; Hathorne & James, 2006; Lemarchand *et al*., 2010; Misra & Froelich, 2012). However, Dellinger *et al*. (2015), through a systematic investigation of modern weathering profiles in the Amazon basin, proposed a more comprehensive "boomerang model", which clarifies the non-monotonic relationship between δ^7Li and weathering intensity. This model has become a key theoretical basis for deep-time paleoweathering reconstructions (Qie *et al*., 2023; Wei *et al*., 2024; Ye *et al*., 2024).

The model divides weathering intensity into three regimes (Fig. 1). The "weathering-limited" regime, characterized by low chemical weathering intensity, is typical of high-altitude mountain belts, where physical erosion dominates, silicate chemical weathering is kinetically limited, and water–rock interaction time is short. It is associated with high dissolved Li flux and low δ^7Li values. Intermediate weathering intensity commonly occurs in trunk rivers and floodplain environments at the mountain–lowland transition. These settings integrate high-altitude erosion and lowland weathering processes. Secondary mineral formation in floodplains induces strong isotope fractionation, producing the highest δ^7Li values, whereas dissolved Li flux decreases due to Li uptake by clay minerals. This stage represents a transitional regime between weathering-limited and supply-limited conditions. High weathering intensity occurs mainly in lowland regions, where physical erosion is weak, the supply of weatherable material is limited, and water–rock interaction time is long. Such settings may yield low δ^7Li values similar to those of high-altitude, low-weathering-intensity regions, but the dissolved Li flux is much lower; this corresponds to a supply-limited weathering regime. Pogge von Strandmann *et al*. (2023) further confirmed the broad applicability of this model across different catchments and showed that lithology modulates the relationship between Li isotopes and weathering intensity by controlling the rate of secondary mineral formation.

How can terrestrial sediments be used to reconstruct continental weathering?

Siliciclastic sediments are important archives for reconstructing catchment-scale weathering processes. Their δ^7Li values mainly reflect the Li isotopic composition of solid terrigenous material, rather than the direct signal of dissolved river water. Because ^{6}Li is preferentially incorporated into solids during secondary clay formation, leaving the residual water relatively enriched in ^{7}Li (Vigier *et al*., 2008; Hindshaw *et al*., 2019), the solid-phase δ^7Li of siliciclastic sediments commonly has an opposite interpretive meaning to dissolved-phase δ^7Li, provided that provenance and grain-size effects remain relatively stable. When the δ^7Li of siliciclastic sediments is close to the average value of the continental crust, it commonly indicates near-congruent weathering of primary silicate minerals or rapid physical erosion, with limited secondary clay formation and weak isotope fractionation. When siliciclastic δ^7Li is lower than the average continental crustal value, it generally indicates the formation of abundant ^{6}Li-enriched secondary clay minerals, reflecting more pronounced incongruent weathering and clay production. In contrast, siliciclastic δ^7Li values higher than the average upper continental crust (UCC) composition pose interpretive challenges and could indicate shifts in provenance toward more radiogenic sources, hydrodynamic grain-size sorting, or admixture of marine authigenic clays that carry a ^{6}Li-

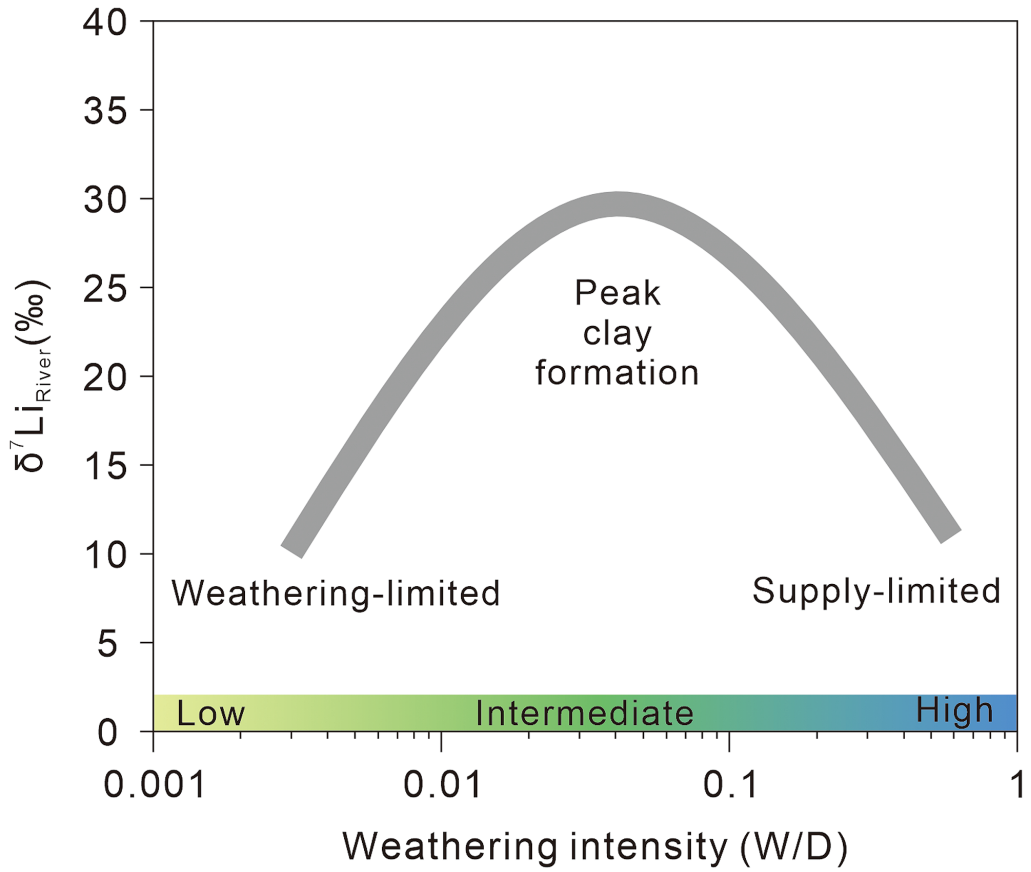

FIGURE 1. The "boomerang model" showing the non-monotonic relationship between riverine δ^7Li and weathering intensity (W/D, chemical weathering / total denudation rate). Proposed by Dellinger *et al*. (2015), this model illustrates the three-stage evolution of dissolved riverine δ^7Li with weathering intensity and serves as the core theoretical foundation for deep-time paleoweathering reconstructions.

depleted signature. Therefore, terrestrial siliciclastic δ^7Li should be interpreted together with provenance, grain size, and sediment-source indicators when reconstructing continental weathering.

During such reconstructions, variations in parent-rock lithology may obscure weathering-intensity signals. Provenance uniformity should be evaluated using immobile-element ratios such as Al_2O_3/TiO_2, Zr/Ti, Th/Sc, and Cr/Th, as well as Th/Sc–Cr/Th and A–CN–K diagrams (McLennan & Taylor, 1991; Hayashi *et al*., 1997; Ye *et al*., 2024). Sediments of different grain sizes also differ in composition. Fine-grained fractions are enriched in secondary clay minerals and commonly have high Li contents and low δ^7Li values, whereas coarse-grained fractions are dominated by relatively unweathered parent-rock debris and show low Li contents and high δ^7Li values (Dellinger *et al*., 2014). Grain-size analysis or proxies such as Al/Si should therefore be used to correct for grain-size effects when interpreting δ^7Li variations. In marine–terrestrial transitional settings, samples may include marine authigenic clay minerals. This effect can be evaluated by examining the linear relationships of Be, Sc, and Th with Al. If these ratios are close to upper-crustal values, the samples can be interpreted as dominated by terrigenous detritus (Wei *et al*., 2020).

Lithium isotopes in marine processes

Three controls on seawater δ^7Li: input, output, and reservoir effects

Seawater δ^7Li is controlled jointly by Li inputs, Li outputs, and the state of the marine Li reservoir (Misra & Froelich, 2012; Li & West, 2014; Sun *et al*., 2018; Cao *et al*., 2022; Qie *et al*., 2023; Rauzi *et al*., 2024; Taylor *et al*., 2026). Therefore, marine δ^7Li records cannot be explained by continental weathering alone, but should be interpreted by distinguishing three types of controls: input control, output control, and reservoir control.

The first is input control, which comprises three end-members: riverine input, hydrothermal input, and subduction-return input (Misra & Froelich, 2012; Sun *et al*., 2018). Because subduction-return input is small and varies slowly over time, its effect on seawater δ^7Li is generally negligible (Sun *et al*., 2018). Therefore, the

main input controls on seawater δ^7Li are the fluxes and isotopic compositions of riverine and hydrothermal Li, represented by F_{riv}, F_{hyd}, δ^7Li_{riv}, and δ^7Li_{hyd}. The riverine input end-member is determined by the continental weathering processes discussed above. Hydrothermal input derives mainly from high-temperature mid-ocean-ridge hydrothermal systems, and its Li isotopic composition is generally much lower than that of modern seawater (Chan *et al*., 1994). Therefore, an increase in hydrothermal Li input can also supply relatively low-δ^7Li Li to the ocean and affect the mass balance of seawater δ^7Li.

The second is output control, which includes mainly basalt alteration and marine authigenic clay formation, *i.e*., reverse weathering (Li & West, 2014; Cao *et al*., 2022; Rauzi *et al*., 2024). Both processes can remove Li from seawater and are accompanied by varying degrees of isotope fractionation. Basalt alteration occurs during seawater–oceanic crust interaction and generally varies little over short timescales. Reverse weathering, in contrast, is more sensitive to environmental change and may exert two opposite effects on seawater δ^7Li. Reverse weathering refers to the formation of authigenic clay minerals (*e.g*., montmorillonite, glauconite) near the sediment-water interface through reactions of dissolved cations with aluminosilicates. Under normal conditions, marine authigenic clay formation preferentially uses light Li from seawater, leaving the residual seawater relatively enriched in ^{7}Li and thereby increasing seawater δ^7Li (Rauzi *et al*., 2024). However, under a scenario of extremely enhanced reverse weathering, the output flux can increase to such an extent that it approaches a near-quantitative removal regime. In this end-member case, the effective isotope fractionation between the authigenic phase and bulk seawater ($\Delta^7Li_{auth\text{-}sw}$) tends toward zero, and the capacity of reverse weathering to elevate seawater δ^7Li collapses. Instead, seawater δ^7Li is driven down toward the integrated isotopic composition of the riverine and hydrothermal inputs.

The third is reservoir control, which includes the size, residence time, and homogenisation state of the marine Li reservoir (Taylor *et al*., 2026). In the modern ocean, Li has a residence time on the order of one million years, much longer than the ocean mixing time. Modern seawater δ^7Li can therefore usually be treated as globally homogeneous. However, if the marine Li reservoir decreases due to reduced inputs or increased outputs, the residence time of Li in the ocean will shorten. Once that residence time approaches the timescale of regional water-mass exchange or ocean mixing, seawater δ^7Li may no longer be fully homogeneous among different oceanic regions, and carbonate, shale, and chert records may show spatial differences.

These three controls can be represented using a first-order marine Li-cycle mass-balance box model (Li & West, 2014; Sun *et al*., 2018; Cao *et al*., 2022; Qie *et al*., 2023; Rauzi *et al*., 2024):

$$\frac{dN_{Li}}{dt} = F_{riv} + F_{hyd} - F_{auth} - F_{alt}$$

where N_{Li} is the marine Li reservoir, F_{riv} is riverine Li input, F_{hyd} is Li input from high-temperature hydrothermal systems, F_{auth} is Li removal through marine authigenic clay formation and reverse weathering, and F_{alt} is Li removal during low-temperature alteration of oceanic crust. The corresponding isotope mass balance can be written as:

$$\frac{d(N_{Li}\delta^7Li_{SW})}{dt} = F_{riv}\delta^7Li_{riv} + F_{hyd}\delta^7Li_{hyd} - F_{auth}\delta^7Li_{auth} - F_{alt}\delta^7Li_{alt}$$

where δ^7Li_{SW}, δ^7Li_{riv}, δ^7Li_{hyd}, δ^7Li_{auth}, and δ^7Li_{alt} represent the Li isotope compositions of seawater, riverine input, hydrothermal input, authigenic removal phases, and low-temperature alteration products, respectively. Because authigenic clay minerals preferentially incorporate ^{6}Li, δ^7Li_{auth} is generally lower than coeval seawater δ^7Li_{SW}. Under near-steady-state conditions:

$$F_{riv} + F_{hyd} = F_{auth} + F_{alt}$$

The residence time of marine Li can be approximated as:

$$\tau_{Li} = \frac{N_{Li}}{F_{auth} + F_{alt}}$$

This model integrates input control, output control, and reservoir control into a single mass-balance framework and shows that the seawater Li reservoir changes according to the difference between input and output fluxes. The residence time of Li in the ocean shortens when the reservoir decreases or when the output flux increases. This framework also indicates that variations in seawater δ^7Li are not controlled by any single end-member alone, but by the coupled effects of input fluxes, output fluxes, isotopic compositions of different end-members, and the size of the marine Li reservoir.

How can marine sediments be used to reconstruct marine δ^7Li?

Marine carbonates are among the most commonly used archives for reconstructing ancient seawater δ^7Li. Because carbonate minerals usually contain low Li concentrations (< 5 ppm; Dellinger *et al*., 2020; Pogge von Strandmann *et al*., 2021), their δ^7Li signals are highly susceptible to diagenesis, terrigenous detrital contamination, and mineralogical variations. Therefore, before carbonate δ^7Li can be used to reconstruct ancient seawater composition, sample preservation must be carefully evaluated. Common screening criteria include Mn/Sr < 3 mmol/mol and δ^{18}O > –10‰, which are used to identify samples that have not experienced strong diagenetic alteration (Banner & Hanson, 1990; Veizer *et al*., 1999; Dellinger *et al*., 2020). Terrigenous detrital contamination can be evaluated using

Al/Ca < 0.8 mmol/mol (Pogge von Strandmann *et al*., 2013; Liu *et al*., 2025), and buffered leaching methods should be used during sample preparation to minimise interference from silicate mineral dissolution in carbonate Li isotope measurements (Cao *et al*., 2023).

When reconstructing seawater δ^7Li, isotope fractionation between carbonate minerals and seawater must also be considered. The Li isotope fractionation factor between carbonate minerals and seawater ($\Delta^7Li_{carb\text{-}sw}$) varies significantly among different carbonate phases. Aragonite shows the strongest fractionation, about –12‰ to –9‰; high-Mg calcite shows intermediate fractionation, about –7‰ to –6‰; and low-Mg calcite and dolomite show the weakest fractionation, about –2‰, meaning that their δ^7Li values are relatively closer to seawater composition (Pogge von Strandmann *et al*., 2019; Dellinger *et al*., 2020; Zhou *et al*., 2025). For biogenic carbonates, such as brachiopod shells and foraminiferal tests, biological effects, shell mineralogy, and preservation state must also be considered because they can further influence Li isotope fractionation (Hathorne & James, 2006; Dellinger *et al*., 2018; Washington *et al*., 2020; Wang *et al*., 2024).

In addition to carbonates, marine shales and cherts can also be used to evaluate the marine Li cycle, but they cannot directly reconstruct ancient seawater δ^7Li (Rauzi *et al*., 2024). Li in marine shales and cherts may derive from both terrigenous detritus and marine authigenic clays. In some sediments, if δ^7Li is far higher than the average value of the continental crust, part of the Li may be derived from marine authigenic clays. Because marine authigenic clay formation generally preferentially incorporates light Li, its δ^7Li is usually lower than coeval seawater. Therefore, such shale and chert records can be used to constrain the minimum value of seawater δ^7Li.

Lithium isotope records across the P–Tr transition: progress, controversies, and new insights

The Permian–Triassic transition is one of the intervals in which Li isotopes have been applied most intensively to deep-time paleoweathering research. Since Sun *et al*. (2018) first reported anomalous seawater δ^7Li near the P–Tr boundary, a series of studies using different archives, sections, and temporal resolutions have emerged, presenting a rich but clearly conflicting picture. This section synthesises the key findings and interpretive frameworks in chronological order of research developments and major controversies.

Early findings: the rapid weathering input hypothesis

Sun *et al*. (2018) reconstructed the seawater δ^7Li evolution near the P–Tr boundary using Li isotope analyses of carbonates and clay minerals from the Global Stratotype Section and Point (GSSP) at Meishan, Zhejiang Province. Their results showed that seawater δ^7Li near the boundary ranged from +8‰ to +18‰, much lower than the modern seawater value (about +31‰). The authors interpreted this low value as evidence of a rapid, massive enhancement of silicate weathering following the STLIP eruption: SO_2 released by volcanism formed acid rain that accelerated the chemical weathering of fresh basalts and volcanic ash, and large amounts of low-δ^7Li river water (close to the mantle value of about +4‰) were rapidly delivered to the ocean, lowering global seawater δ^7Li.

This was the first study to introduce Li isotopes into P–Tr event research, establishing the basic paradigm that "low marine δ^7Li originates from enhanced weathering," a view supported by some subsequent studies. For example, Li isotope data from marine carbonates also show generally low δ^7Li values from the Late Permian to the Early Triassic (Taylor *et al*., 2026), consistent with the rapid weathering-input framework.

Rise of the marine reverse weathering dominance hypothesis

As the studied interval expanded from the immediate P–Tr boundary to the entire Lopingian–Early Triassic interval, more complete seawater δ^7Li curves revealed a more complex long-term evolution than a simple negative excursion. Cao *et al*. (2022), based on carbonate Li isotope data from multiple sections in South China, found that seawater δ^7Li remained relatively stable (about +15‰ to +20‰) for most of the Permian, then declined continuously from the Lopingian (Wuchiapingian) onward and remained anomalously low (about +5‰ to +10‰) throughout the Early Triassic, gradually recovering in the Middle Triassic.

Using box-model inversions, Cao *et al*. (2022) argued that enhanced riverine input alone could not sustain such a long-lasting low-δ^7Li state. They proposed that enhanced marine reverse weathering was the key mechanism driving the Early Triassic low seawater δ^7Li.

Rauzi *et al*. (2024), studying marine shales and cherts, also concluded that reverse weathering was enhanced, but the direction of the δ^7Li change they observed was opposite to that reported by Cao *et al*. (2022). They found that Early Triassic seawater δ^7Li was significantly higher than in the Lopingian, which they attributed to enhanced reverse weathering, on the basis that reverse weathering removed large amounts of light Li, leaving the residual seawater relatively enriched in ^{7}Li. This discrepancy may arise from different archives recording the true seawater signal differently, or it may reflect spatial heterogeneity in the marine Li cycle during the Early Triassic. Crucially, both scenarios highlight that reverse weathering can drive δ^7Li either downward or upward, depending on whether the authigenic clays quantitatively strip most Li from a local water mass (leaving the residual depleted in ^{7}Li) or

merely remove a light Li fraction (leaving the residual enriched). Distinguishing these two modes requires independent constraints on local Li concentrations and burial fluxes.

Direct constraints from terrestrial records: re-evaluating chemical weathering enhancement

The interpretations of the marine records above rely on the assumption that "changes in seawater δ^7Li mainly reflect changes in global continental weathering input" or "changes in reverse weathering." However, directly extracting catchment-scale Li isotope signals from terrestrial sedimentary sequences can provide independent evidence of changes in weathering intensity that are unaffected by internal oceanic processes.

Ye *et al*. (2024) conducted high-resolution paired Li isotope and CIA analyses of clastic rocks spanning terrestrial to marine-terrestrial transitional facies across the P–Tr transition in southwestern China. Their results showed that sediment δ^7Li did not decrease as expected during the extinction interval and into the earliest Early Triassic; instead, it increased significantly in some intervals. Concurrently, CIA indicated a decrease rather than an increase in chemical weathering intensity. Based on these observations, the authors proposed that the weathering regime in southwestern China during the P–Tr transition was characterised by intensified physical erosion and suppressed chemical weathering. The mechanistic explanation is that enhanced hydrological cycling and vegetation destruction caused by large-scale volcanism increased surface runoff and physical denudation, shortened water-rock interaction times, limited full chemical weathering, and thus produced low chemical weathering intensity (low CIA) but high denudation flux.

This finding presents an important challenge to the "global chemical weathering enhancement" hypothesis of Sun *et al*. (2018), revealing that the weathering response at the P–Tr transition may have been strongly heterogeneous in space—different latitudes and paleogeographic settings may have experienced markedly different directions and magnitudes of change in weathering intensity and flux.

Latest challenge: shaking the assumption of seawater δ^7Li homogeneity

All the marine-record studies discussed above share a common assumption: the oceanic residence time of Li is much longer than the mixing time (Pogge von Strandmann *et al*., 2013; Adiatma *et al*., 2024). As a result, seawater δ^7Li is approximately globally homogeneous, and δ^7Li records from any single marine section can represent the global seawater signal. However, a recent study by Taylor *et al*. (2026) has fundamentally questioned this premise.

Taylor *et al*. (2026) systematically compared Li isotope data from different paleoceanographic regions and sedimentary archives (carbonates, shales, cherts) from the Early Triassic and found that the maximum seawater δ^7Li value reconstructed from carbonates was lower than the minimum value reconstructed from shales and cherts. This implies that if each archive accurately recorded the seawater Li isotope composition at the time of deposition, Early Triassic seawater δ^7Li exhibited significant spatial gradients and was far from homogeneous. The authors further proposed that the most likely cause of this heterogeneity was a dramatic shrinkage of the Early Triassic marine Li reservoir. The disappearance of chert deposition at the end of the Permian indicates that, in the context of massive silicifier extinction, marine reverse weathering became unprecedentedly intense, with authigenic clays forming and being buried in large quantities, leading to a sharp drop in seawater Li concentration and a shortening of Li residence time to such an extent that the ocean could no longer fully homogenise Li. Under these conditions, regional differences in Li input and output could not be smoothed out, and seawater δ^7Li exhibited strong local characteristics.

If the hypothesis of Taylor *et al*. (2026) holds, it carries profound methodological implications: (1) δ^7Li records from a single marine section can no longer be treated as equivalent to the global seawater signal; multi-section, multi-archive integrated analysis is necessary. (2) The low or high δ^7Li values of the Early Triassic may reflect local marine Li budgets rather than solely changes in global continental weathering input. (3) The perturbation of the marine Li cycle at the P–Tr transition may have been more complex and stronger than previously recognised.

Synthesis of existing controversies

Table 1 and Fig. 2 summarise the core information and interpretive differences of the main P-Tr Li isotope studies.

In summary, the core controversies currently facing P-Tr Li isotope research can be distilled into three issues:

Controversy 1: Source of the signal—continental weathering *vs.* internal oceanic processes. Does the marine δ^7Li record primarily reflect changes in the δ^7Li and flux of riverine Li input, or is it mainly controlled by fluctuations in the strength of the marine reverse weathering sink? Or do the two alternate in dominance over time?

Controversy 2: Weathering mode—chemical weathering enhancement *vs.* physical erosion enhancement. On a global scale, did continental weathering across the P–Tr transition exhibit a significant increase in chemical leaching intensity (high W/D) or a sharp increase in denudation flux with limited chemical weathering intensity (low to moderate W/D)?

Controversy 3: Nature of the record—globally homogeneous *vs.* locally heterogeneous signal. Can

TABLE 1. Comparison of major P-Tr Li isotope studies.

Archive	Representative study	Method / signal	Main δ^7Li characteristics	Main interpretation	Significance for comparison
Marine carbonate/ clay	Sun *et al*. (2018)	Whole-rock dissolution; siliciclastic correction	Significantly lower than modern near PTB	Rapid chemical weathering enhancement	Represents the "chemical weathering enhancement" view
Marine carbonate	Cao *et al*. (2022)	Sequential leaching	Persistently low from Lopingian to Early Triassic	Extreme marine reverse weathering	P-Tr marine δ^7Li perturbation not necessarily land-controlled
Marine shale/chert	Rauzi *et al*. (2024)	Shale/chert lower-bound constraint on seawater δ^7Li	Early Triassic δ^7Li higher than Lopingian	Enhanced reverse weathering	Opposite direction to Cao *et al*. (2022); reverse weathering effect debated
Terrestrial clastic rock	Ye *et al*. (2024)	Solid-phase weathering signal	Post-extinction δ^7Li is higher than pre-extinction	Physical erosion enhanced; chemical weathering suppressed	Direct evidence of regional "intensity-flux decoupling"
Multi-archive marine	Taylor *et al*. (2026)	Sequential leaching	Carbonate-constrained $\delta^7Li_{SW\text{-}max}$ < clastic-constrained $\delta^7Li_{SW\text{-}min}$	Marine Li reservoir decreased; homogeneity disrupted	Challenges seawater homogeneity premise

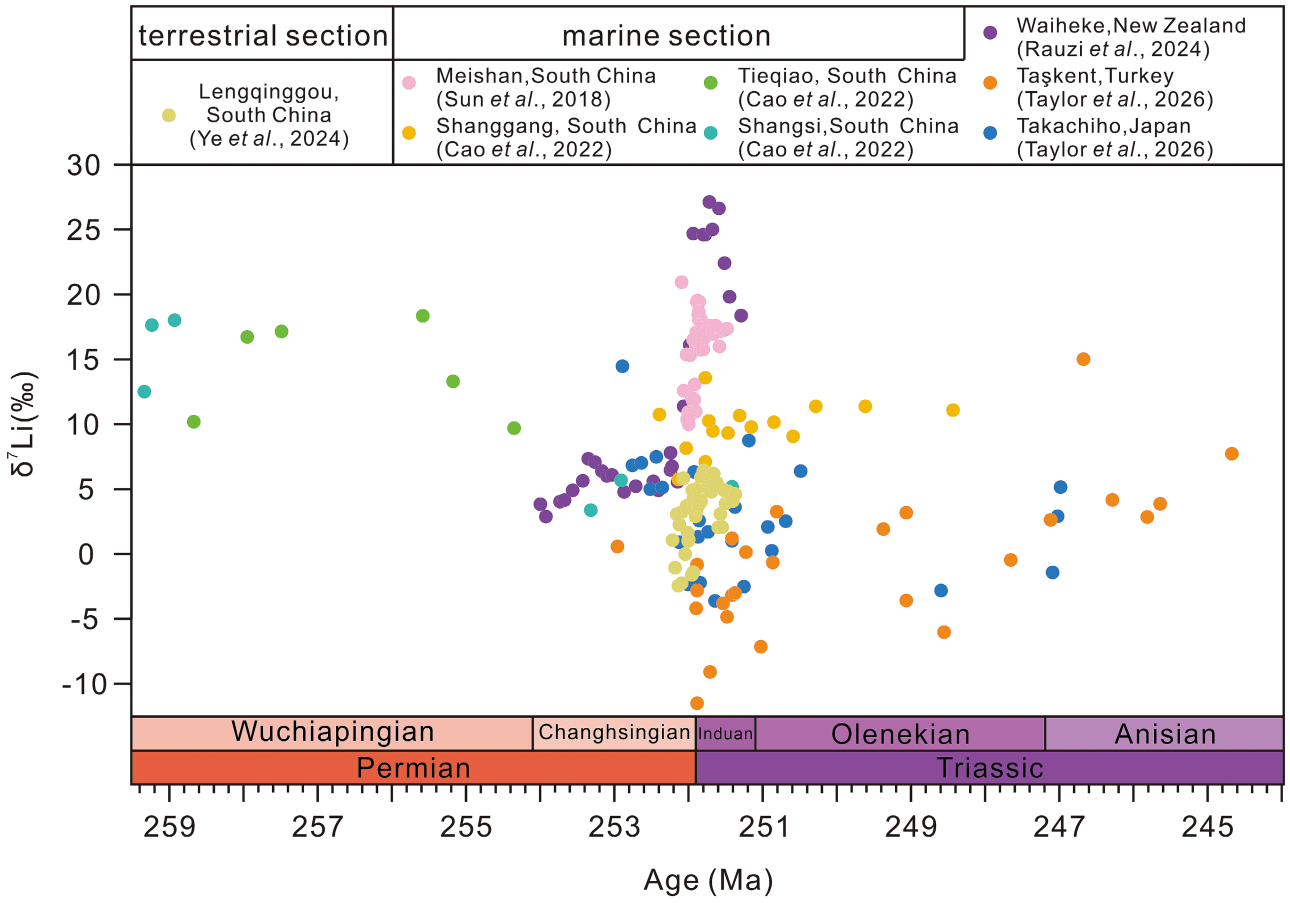

FIGURE 2. Compilation of lithium isotope records from global terrestrial and marine Permian–Triassic sections. Data from Sun *et al*. (2018), Cao *et al*. (2022), and Rauzi *et al*. (2024) are shown as reconstructed seawater δ^7Li values. Data from Taylor *et al*. (2026) are plotted as carbonate δ^7Li values, and data from Ye *et al*. (2024) represent δ^7Li values of core samples from a terrestrial section.

marine δ^7Li records still represent the global seawater reservoir during the Early Triassic? Have local variations in the marine Li budget become large enough to overwhelm the global weathering signal?

Resolving these controversies cannot rely solely on the interpretation of a single proxy (Li isotopes); it is necessary to place them within a comparative framework that includes other weathering proxies (CIA, Sr, Os, Mg isotopes) and to conduct systematic deconvolution analysis using numerical models.

Multi-proxy comparison and integrated analysis: from divergence to synergy

Because of their distinct geochemical behaviours, response timescales, and sensitivities to post-depositional preservation, different weathering proxies often record different facets of the same geological event. In P–Tr weathering research, relying on a single proxy (Li isotopes) cannot resolve the three-fold controversy (signal source, weathering mode, homogeneity). A systematic comparison and deconvolution of δ^7Li with the Chemical Index of Alteration (CIA), Sr isotopes, Os isotopes, and Mg isotopes are critical for identifying the "greatest common denominator" that all proxies agree on and to understand the specific differences among them.

Major- and trace-element weathering indices: direct records of chemical alteration intensity

The Chemical Index of Alteration (CIA) and its corrected form ($CIA_{(corr.)}$) directly indicate the degree of chemical weathering experienced by source rocks by quantifying leaching of mobile alkali elements (Na, K, Ca) relative to immobile Al in aluminosilicate minerals such as feldspars (Nesbitt & Young, 1982; Fedo *et al*., 1995). Here, we use CIA primarily as a proxy for chemical weathering intensity, *i.e*., the degree of source-area chemical alteration. Unlike isotopic proxies, CIA is unaffected by internal oceanic processes and reflects local catchment-scale weathering signals.

The global compilation of CIA and $CIA_{corr.}$ data from P–Tr terrigenous clastic rocks by Xu *et al*. (2023) shows that during the peak extinction interval through the earliest Early Triassic, silicate chemical weathering intensity did not increase significantly at most sections globally; instead, it showed a decreasing trend. The paired analysis of the terrestrial section in southwestern China by Ye *et al*. (2024) further confirms that the extinction interval was characterised by a decline in CIA accompanied by an increase in physical sedimentation rate, indicating a shift to a weathering regime of enhanced physical erosion and suppressed chemical weathering. This result directly contradicts the "global chemical weathering enhancement" hypothesis proposed by Sun *et al*. (2018) based on marine δ^7Li.

The contradiction between the two proxies reveals a key insight: CIA records the degree of chemical alteration, whereas marine δ^7Li reflects the flux-weighted average isotopic composition of riverine Li input. In a context of vegetation destruction, exposed land surfaces, and sharply increased runoff coefficients, even if the chemical alteration experienced by each unit mass of rock is limited (low CIA), the rapid erosion of large volumes of fresh detrital material can still generate a considerable dissolved Li flux. Moreover, because water-rock interaction times are short, the δ^7Li of this flux tends to be low. Therefore, the contradiction between CIA and marine δ^7Li precisely indicates the decoupling of chemical weathering intensity and physical denudation flux at the P–Tr transition, rather than the failure of either proxy.

Sr isotopes: independent evidence for increased terrigenous input flux

The seawater $^{87}Sr/^{86}Sr$ ratio is a classic proxy for reconstructing changes in continental weathering input over geological history. The oceanic residence time of Sr (~2–3 Myr) is longer than the ocean mixing time (Capo *et al*., 1998), so the global seawater Sr isotope composition is relatively homogeneous. Its variations primarily reflect changes in the radiogenic Sr input from continental sources (mainly weathering of old silicate rocks) relative to non-radiogenic Sr from mantle sources (mid-ocean ridge hydrothermal fluids and island-arc volcanism) (Palmer & Edmond, 1989; Pearce *et al*., 2015; Peucker-Ehrenbrink & Fiske, 2019). The radiogenic Sr input is mainly controlled by both the magnitude of continental weathering flux and the Sr isotopic composition of the weathered source rocks (Chen *et al*., 2021; Zhao *et al*., 2025).

The global seawater $^{87}Sr/^{86}Sr$ curve across the P–Tr transition shows a continuous, significant rise, from about 0.7070 in the Late Permian to 0.7071–0.7083 in the Early Triassic (Korte *et al*., 2003, 2006; Dudás *et al*., 2017; Wang *et al*., 2021). This trend is widely interpreted as reflecting a substantial increase in continental weathering flux, with the injection of large amounts of radiogenic Sr overwhelming any contemporaneous increase in mantle-derived input (Korte *et al*., 2003; Sedlacek *et al*., 2014; Song *et al*., 2015; Dudás *et al*., 2017; Wang *et al*., 2019, 2021; Cao *et al*., 2022; Garbelli *et al*., 2022; Liu *et al*., 2023).

Unlike Li isotopes, $^{87}Sr/^{86}Sr$ cannot distinguish between silicate and carbonate weathering contributions, nor does it directly indicate changes in chemical weathering intensity. An increase in physical denudation alone could deliver more terrigenous Sr-bearing material to the ocean without requiring stronger chemical leaching. Crucially, the $^{87}Sr/^{86}Sr$ mass balance is also sensitive to lithology, as the weathering of radiogenic felsic rocks versus less radiogenic mafic or carbonate lithologies can produce divergent Sr signals even under identical weathering fluxes (Chen *et al*., 2021; Zhao *et al*., 2025). Therefore,

while indicative of an overall increase in crustal input, the Sr record alone cannot distinguish lithological shifts from changes in the total weathering flux. Nevertheless, comparison between Sr and Li isotopes provides two useful constraints. (1) The Early Triassic rise in seawater $^{87}Sr/^{86}Sr$ indicates an increased contribution of continental Sr to the ocean over a relatively integrated timescale, although the exact source lithology and weathering pathway remain uncertain. (2) When considered together with Li isotope and CIA records (Xu *et al*., 2023; Ye *et al*., 2024), the Sr isotope trend suggests that enhanced terrigenous input did not necessarily correspond to stronger source-area chemical alteration. Instead, it is more consistent with a weathering regime characterized by increased physical denudation and material supply, but limited chemical weathering intensity.

Os isotopes: high-resolution records of the volcanic-weathering transition

The osmium (Os) isotope system ($^{187}Os/^{188}Os$) is similar to Sr isotopes in that it exhibits a large isotopic contrast between the weathering end-member (old continental crust, highly radiogenic) and the volcanic/hydrothermal end-member (mantle/cosmogenic, unradiogenic) (Peucker-Ehrenbrink & Ravizza, 2000; Cohen *et al*., 2004; Georg *et al*., 2013). The key advantage of Os is its extremely short oceanic residence time (~10^4 years) (Peucker-Ehrenbrink & Ravizza, 2000; Rooney *et al*., 2016), which allows it to record rapid environmental perturbations on millennial to ten-thousand-year timescales without being smoothed out by the long oceanic buffering effect.

The $^{187}Os/^{188}Os$ record across the P–Tr transition exhibits a clear three-stage evolution (Schoepfer *et al*., 2013; Georgiev *et al*., 2015, 2020; Liu *et al*., 2020; Liu & Selby, 2021; Nsingi *et al*., 2025):

Stage 1 (pre-extinction to early extinction): $^{187}Os/^{188}Os$ drops sharply to about 0.3–0.4, reflecting a pulsed injection of unradiogenic Os during the main eruptive phase of the STLIP and directly recording the peak intensity of volcanic activity.

Stage 2 (near PTB to early Early Triassic): The ratio rebounds rapidly to >1.0 within a few hundred thousand years, indicating a sharp increase in continental weathering flux as volcanic input waned, with weathering rates reaching a peak.

Stage 3 (middle to late Early Triassic): The ratio returns to pre-extinction levels, possibly reflecting a decline in weathering flux or a decrease in weathering intensity as atmospheric pCO_2 declines.

Compared with Li isotopes, the Os isotope system is largely unaffected by internal oceanic reverse-weathering processes because Os behaves conservatively in the ocean and its uptake by authigenic sediments does not produce significant isotope fractionation (Peucker-Ehrenbrink & Ravizza, 2000). Therefore, the Os isotope record unambiguously indicates that the continental weathering flux at the P–Tr transition experienced a rapid onset, a peak increase, and a gradual decline. The complexity of the Li isotope record (*e.g*., differences among archives in the Early Triassic) is more likely to arise from modulation by the internal marine Li cycle (reverse weathering, reservoir size changes) rather than from a persistently low continental weathering flux (Cao *et al*., 2022; Rauzi *et al*., 2024; Taylor *et al*., 2026).

Mg isotopes: combined constraints from secondary minerals and dolomitization

Magnesium (Mg) isotopes ($\delta^{26}Mg$), like Li isotopes, are non-traditional stable isotopes that undergo significant fractionation during secondary mineral formation. The overall fractionation paths of Mg and Li share similarities and differences. During silicate dissolution, Mg is released incongruently, with light Mg preferentially entering the water (Tipper *et al*., 2006), whereas Li shows almost no fractionation during source rock dissolution (Pogge von Strandmann *et al*., 2013; Dellinger *et al*., 2015; Hindshaw *et al*., 2019). During secondary mineral formation, ^{26}Mg is preferentially incorporated, causing fractionation. As weathering intensifies, secondary minerals enriched in ^{26}Mg dissolve preferentially, leaving the residual phase with light Mg signatures (Tipper *et al*., 2006; Pogge von Strandmann *et al*., 2008; Huang *et al*., 2024). Some studies also show that Mg isotope fractionation during secondary mineral dissolution is mineral-specific (Wimpenny *et al*., 2010) and varies among binding sites (Wimpenny *et al*., 2014). In addition, dolomitization is an important control on Mg isotope fractionation: during dolomite formation, light ^{24}Mg preferentially enters the lattice, while heavy ^{26}Mg remains in the fluid (Hu *et al*., 2021).

In weathering tracing, Mg isotopes provide complementary constraints to Li isotopes. The two share similar fractionation paths during secondary mineral formation but differ significantly in processes such as dolomitization and internal oceanic cycling; thus, their combined analysis can constrain different aspects. Furthermore, Mg has an extremely long oceanic residence time (~13 Ma) (Ling *et al*., 2011); short-term variations in $\delta^{26}Mg$ can test for basin restriction and provide a reference for whether Li isotopes represent a global signal.

Existing P–Tr marine carbonate Mg isotope data show a positive shift of about 0.4‰ in $\delta^{26}Mg$ near the PTB (Hu *et al*., 2021). This change is interpreted as resulting from enhanced continental weathering and widespread

dolomitization. Enhanced weathering delivered river water enriched in $\delta^{26}Mg$ to the ocean, while dolomitization under extreme greenhouse conditions further removed light Mg from seawater, raising the $\delta^{26}Mg$ of the residual seawater. The rapid change in $\delta^{26}Mg$ also implies a brief restricted-basin event in the Paleotethys Ocean, consistent with the latest inferences from Li isotopes (Taylor *et al*., 2026). In the Early Triassic, the average $\delta^{26}Mg$ of marine siliciclastic sediments increased by about 1.5‰, interpreted as reflecting intense chemical weathering driven by CO_2 degassing and climate warming (Chen *et al*., 2020).

Multi-proxy deconvolution: three-dimensional separation of weathering intensity, flux, and oceanic processes

By synthesising the characteristics of the five proxy types (Li, CIA, Sr, Os, Mg), the environmental signals related to weathering across the P–Tr transition can be decomposed into three interrelated yet separable dimensions (Table 2).

Three-dimensional deconvolution model (schematic in Fig. 3) can be summarised as:

(1) Intensity dimension (constrained by CIA): In most terrestrial regions globally, silicate chemical weathering intensity at the P–Tr transition did not increase linearly

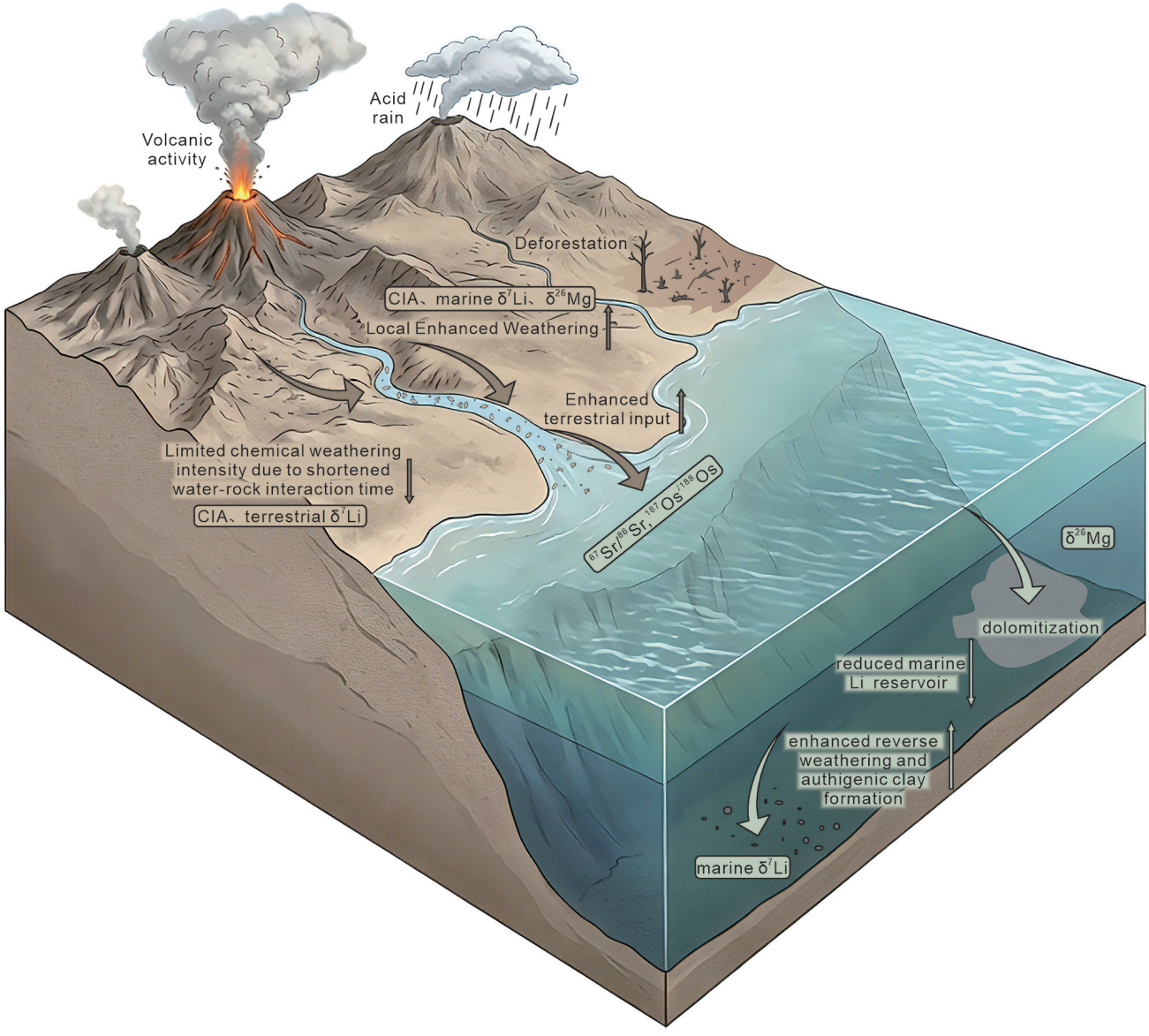

FIGURE 3. Schematic diagram of the "intensity-flux decoupling" model of continental weathering and multi-proxy responses across the Permian–Triassic transition. Volcanic activity triggered vegetation collapse and a shortened hydrological cycle, leading to a decoupled weathering regime characterized by enhanced physical erosion but limited chemical weathering intensity. Multiple proxies record weathering intensity, terrigenous input flux, and key marine processes including enhanced reverse weathering and a reduced marine Li reservoir. Straight arrows indicate trends in flux or reservoir changes; upward arrows denote increases, whereas downward arrows denote decreases. Curved arrows indicate the direction of material transport.

TABLE 2. Multi-proxy decomposition of weathering signals at the P–Tr transition.

Dimension	Main constraining proxies	Overall P–Tr characteristic	Significance
Weathering intensity	CIA, $\delta^{26}Mg$, $\delta^{7}Li$ (terrestrial)	Largely unchanged or decreased in most regions; increased in a few regions	Local chemical weathering degree is limited; water-rock interaction time is shortened
Terrigenous input flux	$^{87}Sr/^{86}Sr$, $^{187}Os/^{188}Os$	Continuously rising or pulsed increase	Total flux of weathering products delivered to the ocean increased markedly
Internal oceanic process	Marine $\delta^{7}Li$	Anomalous low, high, or spatially heterogeneous values	Reverse weathering is an important climate modulator

with temperature (Chen *et al*., 2022; Xu *et al*., 2023; Ye *et al*., 2024). The shortening of the hydrological cycle (rapid runoff) and the acceleration of physical denudation caused by vegetation collapse (Feng *et al*., 2020; Wu *et al*., 2021) compressed the time window for chemical weathering, reducing the degree of leaching per unit rock. The mechanistic chain is further elucidated as follows: volcanic CO_2-driven warming, coupled with wildfire activity, destabilizes terrestrial carbon reservoirs and vegetation cover. SO_2-derived acid rain and sulfate deposition impose an additional chemical stressor, enhancing cation leaching from foliage and soils (Zhang *et al*., 2023; Chen *et al*., 2025). The resulting vegetation and root systems collapse eliminates soil-binding agents, drastically reduces biologically-mediated weathering, and promotes rapid, unconfined runoff. Consequently, the system shifts to a regime dominated by soil stripping and detrital export, where material flux to the ocean increases, but the mean water–rock interaction time is insufficient for significant chemical leaching. This scenario provides a direct mechanistic link between terrestrial ecosystem breakdown and the observed intensity–flux decoupling.

(2) Flux dimension (constrained by Sr, Os): Although chemical weathering intensity was limited, the exposure and water-rock interaction of vast amounts of fresh rock during rapid physical denudation still led to a substantial increase in the total flux of dissolved weathering products (Algeo & Twitchett, 2010). The Os isotope record further constrains the timing of the onset and the peak interval of this flux surge (Liu *et al*., 2020; Liu & Selby, 2021).

(3) Oceanic dimension (constrained by marine Li): Marine reverse weathering was anomalously enhanced under the extreme greenhouse-anoxic conditions of the Early Triassic, and its effect on Li removal overwhelmingly shaped the seawater $\delta^{7}Li$ signal (Cao *et al*., 2022; Rauzi *et al*., 2024). In addition, the possible shrinkage of the Li reservoir (Taylor *et al*., 2026) further complicates the global representativeness of marine records.

This deconvolution framework reconciles several previously seemingly contradictory observations: the rapid $\delta^{7}Li$ decrease near the PTB observed by Sun *et al*. (2018) may have resulted from both isotopically light riverine input and enhanced reverse weathering. The long-term low $\delta^{7}Li$ recorded by Cao *et al*. (2022) more strongly reflects internal oceanic effects of persistent reverse weathering and a shrinking marine Li reservoir. The regime of enhanced physical erosion and suppressed chemical weathering revealed by Ye *et al*. (2024) provides a direct constraint on the local weathering intensity dimension. These three are not mutually exclusive but capture different facets of the Earth surface system's response during the P–Tr upheaval.

A practical illustration of this deconvolution can be drawn from the South China records. At Meishan, the sharp $\delta^{7}Li$ drop (Sun *et al*., 2018) coincides with Os evidence for volcanic onset and the initial weathering pulse (Liu *et al*., 2020). However, the persistently low $\delta^{7}Li$ in the overlying Early Triassic strata (Cao *et al*., 2022) occurs when Os ratios already indicate declining terrigenous flux. Without the reverse-weathering dimension, the prolonged

TABLE 3. Oceanic residence times and response scales of weathering proxies.

Proxy	Oceanic residence time	Response timescale	Main contribution to P-Tr research
CIA	–	Transient (stratigraphic resolution)	Direct record of local chemical weathering intensity
$^{187}Os/^{188}Os$	~10^4 yr	Millennial	Constrains onset and peak timing of the weathering flux surge
$\delta^{7}Li$	~1-1.5 Ma (normal); variable	Million-year (normally); can be shorter	Indicates the balance between weathering input and reverse weathering
$^{87}Sr/^{86}Sr$	~2–3 Ma	Hundred-thousand to million-year	Indicates the long-term trend in total terrigenous input flux
$\delta^{26}Mg$	~13 Ma	Ten-million-year	Weathering input changes in restricted basins

low δ^7Li would imply continuous high weathering flux, contradicting Os. With the three-dimensional framework, the low δ^7Li can be understood as the oceanic response to persistent reverse weathering and a shrinking reservoir, superimposed on a declining weathering flux. This example underscores how multi-proxy deconvolution turns apparent contradictions into a coherent narrative.

Timescale differences among proxies and their significance for integration

Differences in temporal resolution and response lag among the various proxies must also be considered when explaining discrepancies (Table 3). Os isotopes, with their very short oceanic residence time, can record weathering pulses on centennial to millennial scales (Peucker-Ehrenbrink & Ravizza, 2000; Rooney *et al*., 2016). Li isotopes, with their long residence time, would normally smooth out short-term signals, but reverse weathering enhancement and reservoir shrinkage can significantly alter their behaviour (Pogge von Strandmann *et al*., 2013; Taylor *et al*., 2026). Sr isotopes, with their longer residence time, record average changes on ten-thousand-year to million-year scales (Capo *et al*., 1998). Mg isotopes record even longer-scale changes, so their significant short-term fluctuations may also serve as an independent indicator of basin restriction (Ling *et al*., 2011; Hu *et al*., 2021).

The proxies thus resolve the event into a coherent temporal sequence: an initial Os isotope minimum marking the volcanic paroxysm is followed within a few hundred thousand years by an Os isotope maximum that records a sharp but transient increase in terrestrial erosion. This weathering pulse is then overprinted in the marine Li isotope record by a strong internal oceanic response, as extreme reverse weathering and a collapsing Li inventory reshape seawater δ^7Li. Ultimately, the long-term climatic consequences are captured by persistently radiogenic Sr isotope ratios, which reflect the protracted re-equilibration of global weathering under elevated atmospheric CO_2. This multiscale perspective is essential because the instantaneous weathering response may be dominated by physical denudation (low CIA, moderate riverine δ^7Li), whereas the long-term integrated signal in the ocean is shaped more strongly by the cumulative effects of reverse weathering and reservoir dynamics.

Conclusion

Main findings

The complexity of P–Tr lithium isotope records reflects the superposition of multiple processes: changes in continental silicate weathering input, enhanced marine reverse weathering, and a possible shrinkage of the marine Li reservoir. Interpretive disagreements among studies stem largely from different weightings of these three factors.

A pronounced "intensity-flux decoupling" characterises continental weathering. CIA and terrestrial δ^7Li indicate that chemical weathering intensity did not increase (or even decreased) globally, whereas Sr-Os isotopes record a sharp rise in terrigenous flux. This contradiction is resolved by a regime of rapid physical erosion with limited chemical leaching, driven by vegetation collapse and acid rain, which shortened water-rock interaction times.

Marine δ^7Li was not a passive record of continental input; it was co-modulated by extreme perturbations of the internal Li cycle—enhanced reverse weathering and a likely reduced Li reservoir. Finally, multi-proxy deconvolution is essential: CIA constrains local intensity, Os captures flux timing, Sr tracks long-term terrigenous flux, Li records weathering-ocean coupling, and Mg provides complementary constraints. Only an integrated framework can reveal the true Earth-surface response.

Outstanding issues and future research directions

Several key bottlenecks remain. Archive effects (offsets among carbonates, shales, cherts, and brachiopods) require quantitative correction via diagenetic experiments and multi-archive cross-checks. Spatial heterogeneity remains poorly constrained; high-resolution paired δ^7Li-CIA studies across latitudes and lithologies are needed to map global weathering intensity. Dynamic numerical modelling of the marine Li cycle—coupling continental weathering, reverse weathering, and burial—is required to separate source and sink contributions to seawater δ^7Li. Higher-resolution coupled terrestrial-marine records, ideally with Li isotope analysis matching Os isotope resolution, can directly link local weathering intensity to global seawater signals. Integration with other volatile cycles (pCO_2, carbon isotopes, temperature, Hg isotopes) will quantify CO_2 drawdown by silicate weathering. Finally, cross-event comparisons (end-Triassic, end-Cretaceous, PETM) can identify universal weathering behaviours and event-specific responses.

In summary, P–Tr weathering research is shifting from qualitative, single-proxy interpretations to quantitative, multi-proxy deconvolution. Li isotopes play a key bridging role. With improved analytical precision, broader spatial coverage, and better models, a unified picture of P–Tr weathering evolution will emerge, offering a key paradigm for understanding deep-time Earth system crises.

Acknowledgements

We sincerely thank the editors and reviewers for

their constructive comments and suggestions, which significantly strengthened this manuscript. This work was supported by the National Natural Science Foundation of China (92479206), the Jiangsu Innovation Support Plan for International Science and Technology Cooperation Program (BZ2023068).

References

Adiatma, Y.D., Saltzman, M.R. & Liu, X.M. (2024) Lithium isotope stratigraphy and Ordovician weathering. *Earth and Planetary Science Letters*, 647, 119030. https://doi.org/10.1016/j.epsl.2024.119030

Algeo, T.J. & Twitchett, R.J. (2010) Anomalous Early Triassic sediment fluxes due to elevated weathering rates and their biological consequences. *Geology*, 38 (11), 1023–1026. https://doi.org/10.1130/G31203.1

Banner, J.L. & Hanson, G.N. (1990) Calculation of simultaneous isotopic and trace element variations during water-rock interaction with applications to carbonate diagenesis. *Geochimica et Cosmochimica Acta*, 54 (11), 3123–3137. https://doi.org/10.1016/0016-7037(90)90128-8

Cao, C., Bataille, C.P., Song, H.J., Saltzman, M.R., Cramer, K.T., Wu, H.C., Korte, C., Zhang, Z.F. & Liu, X.M. (2022) Persistent late Permian to Early Triassic warmth linked to enhanced reverse weathering. *Nature Geoscience*, 15, 832–838. https://doi.org/10.1038/s41561-022-01078-y

Cao, C., Liu, X.M., Wang, X.K. & Chen, J. (2023) Effective use of limestones to reconstruct seawater Li isotope compositions—a community standard proposal. *Chemical Geology*, 626, 121441. https://doi.org/10.1016/j.chemgeo.2023.121441

Cao, Y., Song, H.Y., Algeo, T.J., Chu, D.L., Du, Y., Tian, L., Wang, Y.H. & Tong, J.N. (2019) Intensified chemical weathering during the Permian-Triassic transition recorded in terrestrial and marine successions. *Palaeogeography, Palaeoclimatology, Palaeoecology*, 519, 166–177. https://doi.org/10.1016/j.palaeo.2018.06.012

Capo, R.C., Stewart, B.W. & Chadwick, O.A. (1998) Strontium isotopes as tracers of ecosystem processes: theory and methods. *Geoderma*, 82 (1-3), 197–225. https://doi.org/10.1016/S0016-7061(97)00102-X

Chan, L.H., Gieskes, J.M., You, C.F. & Edmond, J.M. (1994) Lithium isotope geochemistry of sediments and hydrothermal fluids of the Guaymas Basin, Gulf of California. *Geochimica et Cosmochimica Acta*, 58 (20), 4443–4454. https://doi.org/10.1016/0016-7037(94)90346-8

Chen, X.Y., Teng, F.Z., Huang, K.J. & Algeo, T.J. (2020) Intensified chemical weathering during Early Triassic revealed by magnesium isotopes. *Geochimica et Cosmochimica Acta*, 287, 263–276. https://doi.org/10.1016/j.gca.2020.02.035

Chen, B., Chen, J., Qie, W., Huang, P., He, T., Joachimski, M.M. & Algeo, T.J. (2021) Was climatic cooling during the earliest Carboniferous driven by expansion of seed plants? *Earth and Planetary Science Letters*, 565, 116953. https://doi.org/10.1016/j.epsl.2021.116953

Chen, J., Guo, Y., Wei, H.B., Liu, H.Y., Ma, R.Y., Xiao, Z. & Feng, Z. (2022) Evaluation of chemical weathering proxies by comparing drilled cores versus outcrops and weathering history during the Permian–Triassic transition. *Global and Planetary Change*, 214, 103855. https://doi.org/10.1016/j.gloplacha.2022.103855

Chen, J.B., Lu, B.J., Du, L.Y., Lin, M., Shen, S.Z., Montañez, I.P. & Feng, Z. (2025) Regional postdeforestation weathering feedback drove diachronous C-S cycle perturbations during the end-Permian crisis. *Proceedings of the National Academy of Sciences*, 122 (44), e2504841122. https://doi.org/10.1073/pnas.2504841122

Clarkson, M.O., Wood, R.A., Poulton, S.W., Richoz, S., Newton, R.J., Kasemann, S.A., Bowyer, F. & Krystyn, L. (2016) Dynamic anoxic ferruginous conditions during the end-Permian mass extinction and recovery. *Nature Communications*, 7, 12236. https://doi.org/10.1038/ncomms12236

Cohen, A.S., Coe, A.L., Harding, S.M. & Schwark, L. (2004) Osmium isotope evidence for the regulation of atmospheric CO2 by continental weathering. *Geology*, 32 (2), 157–160. https://doi.org/10.1130/G20158.1

Dal Corso, J., Song, H.J., Callegaro, S., Chu, D.L., Sun, Y.D., Hilton, J., Grasby, S.E., Joachimski, M.M. & Wignall, P.B. (2022) Environmental crises at the Permian–Triassic mass extinction. *Nature Reviews Earth & Environment*, 3, 197–214. https://doi.org/10.1038/s43017-021-00259-4

Dellinger, M., Gaillardet, J., Bouchez, J., Calmels, D., Galy, V., Hilton, R.G., Louvat, P. & France-Lanord, C. (2014) Lithium isotopes in large rivers reveal the cannibalistic nature of modern continental weathering and erosion. *Earth and Planetary Science Letters*, 401, 359–372. https://doi.org/10.1016/j.epsl.2014.05.061

Dellinger, M., Gaillardet, J., Bouchez, J., Calmels, D., Louvat, P., Dosseto, A., Gorge, C., Alanoca, L. & Maurice, L. (2015) Riverine Li isotope fractionation in the Amazon River basin controlled by the weathering regimes. *Geochimica et Cosmochimica Acta*, 164, 71–93. https://doi.org/10.1016/j.gca.2015.04.042

Dellinger, M., Hardisty, D.S., Planavsky, N.J., Gill, B.C., Kalderon-Asael, B., Asael, D., Croissant, T., Swart, P.K. & West, A.J. (2020) The effects of diagenesis on lithium isotope ratios of shallow marine carbonates. *American Journal of Science*, 320 (2), 150–184. https://doi.org/10.2475/02.2020.03

Dellinger, M., West, A.J., Paris, G., Adkins, J.F., Pogge von Strandmann, P.A.E., Ullmann, C.V., Eagle, R.A., Freitas, P., Bagard, M.L., Ries, J.B., Corsetti, F.A., Perez-Huerta, A. & Kampf, A.R. (2018) The Li isotope composition of marine

biogenic carbonates: Patterns and mechanisms. *Geochimica et Cosmochimica Acta*, 236, 315–335. https://doi.org/10.1016/j.gca.2018.03.014

Dudás, F., Yuan, D.X., Shen, S.Z. & Bowring, S.A. (2017) A conodont-based revision of the 87Sr/86Sr seawater curve across the Permian-Triassic boundary. *Palaeogeography, Palaeoclimatology, Palaeoecology*, 470, 40–53. https://doi.org/10.1016/j.palaeo.2017.01.007

Fan, J.X., Shen, S.Z., Erwin, D.H., Sadler, P.M., MacLeod, N., Cheng, Q.M., Hou, X.D., Yang, J., Wang, X.D., Wang, Y., Zhang, H., Chen, X., Li, G.X., Zhang, Y.C., Shi, Y.K., Yuan, D.X., Chen, Q., Zhang, L.N., Li, C. & Zhao, Y.Y. (2020) A high-resolution summary of Cambrian to Early Triassic marine invertebrate biodiversity. *Science*, 367 (6475), 273–277. https://doi.org/10.1126/science.aax4953

Fedo, C.M., Nesbitt, H.W. & Young, G.M. (1995) Unraveling the effects of potassium metasomatism in sedimentary rocks and paleosols, with implications for paleoweathering conditions and provenance. *Geology*, 23 (10), 921–924. https://doi.org/10.1130/0091-7613(1995)023<0921:UTEOPM>2.3.CO;2

Feng, Z., Wei, H.B., Guo, Y., He, X.Y., Sui, Q., Zhou, Y., Liu, H.Y., Gou, X.D. & Lv, Y. (2020) From rainforest to herbland: New insights into land plant responses to the end-Permian mass extinction. *Earth-Science Reviews*, 204, 103153. https://doi.org/10.1016/j.earscirev.2020.103153

Garbelli, C., Cipriani, A., Brand, U., Lugli, F. & Posenato, R. (2022) Strontium isotope stratigraphic insights on the end-Permian mass extinction and the Permian-Triassic boundary in the Dolomites (Italy). *Chemical Geology*, 605, 120946. https://doi.org/10.1016/j.chemgeo.2022.120946

Georg, R.B., West, A.J., Vance, D., Newman, K. & Halliday, A.N. (2013) Is the marine osmium isotope record a probe for CO2 release from sedimentary rocks? *Earth and Planetary Science Letters*, 367, 28–38. https://doi.org/10.1016/j.epsl.2013.02.018

Georgiev, S.V., Stein, H.J., Hannah, J.L., Henderson, C.M. & Algeo, T.J. (2015) Enhanced recycling of organic matter and Os-isotopic evidence for multiple magmatic or meteoritic inputs to the Late Permian Panthalassic Ocean, Opal Creek, Canada. *Geochimica et Cosmochimica Acta*, 150, 192–210. https://doi.org/10.1016/j.gca.2014.11.019

Georgiev, S.V., Stein, H.J., Yang, G., Hannah, J.L., Böttcher, M.E., Grice, K., Holman, A., Turgeon, S., Simonsen, S. & Cloquet, C. (2020) Late Permian-Early Triassic environmental changes recorded by multi-isotope (Re-Os-N-Hg) data and trace metal distribution from the Hovea-3 section, Western Australia. *Gondwana Research*, 88, 353–372. https://doi.org/10.1016/j.gr.2020.07.007

Hathorne, E. & James, R. (2006) Temporal record of lithium in seawater: A tracer for silicate weathering? *Earth and Planetary Science Letters*, 246 (3-4), 393–406. https://doi.org/10.1016/j.epsl.2006.04.020

Hayashi, K., Fujisawa, H., Holland, H.D. & Ohmoto, H. (1997) Geochemistry of similar to 1.9 Ga sedimentary rocks from northeastern Labrador, Canada. *Geochimica et Cosmochimica Acta*, 61 (19), 4115–4137. https://doi.org/10.1016/S0016-7037(97)00214-7

Hindshaw, R.S., Tosca, R., Goût, T.L., Farnan, I., Tosca, N.J. & Tipper, E.T. (2019) Experimental constraints on Li isotope fractionation during clay formation. *Geochimica et Cosmochimica Acta*, 250, 219–237. https://doi.org/10.1016/j.gca.2019.02.015

Hu, Z.Y., Li, W.Q., Zhang, H., Krainer, K., Zheng, Q.F., Xia, Z.G., Hu, W.X. & Shen, S.Z. (2021) Mg isotope evidence for restriction events within the Paleotethys ocean around the Permian-Triassic transition. *Earth and Planetary Science Letters*, 556, 116704. https://doi.org/10.1016/j.epsl.2020.116704

Huang, T.Z., Shen, B., Huang, K.J., Ning, M., Li, C., Xue, J.Z., Sun, Y.L. & Huang, B.Q. (2024) Revisiting the Mg isotopic systematics of siliciclastic components of sediments and sedimentary rocks: A new geochemical proxy of continental weathering in Earth's history. *Science China-Earth Sciences*, 67 (2), 620–633. https://doi.org/10.1007/s11430-023-1199-2

Huh, Y., Chan, L.H. & Edmond, J.M. (2001) Lithium isotopes as a probe of weathering processes: Orinoco River. *Earth and Planetary Science Letters*, 194 (1-2), 189–199. https://doi.org/10.1016/S0012-821X(01)00523-4

Jiao, S.L., Zhang, H., Cai, Y.F., Chen, J.B., Feng, Z. & Shen, S.Z. (2023) Collapse of tropical rainforest ecosystems caused by high-temperature wildfires during the end-Permian mass extinction. *Earth and Planetary Science Letters*, 614, 118193. https://doi.org/10.1016/j.epsl.2023.118193

Joachimski, M.M., Lai, X., Shen, S., Jiang, H., Luo, G., Chen, B., Chen, J. & Sun, Y. (2012) Climate warming in the latest Permian and the Permian-Triassic mass extinction. *Geology*, 40 (3), 195–198. https://doi.org/10.1130/G32707.1

Jurikova, H., Gutjahr, M., Wallmann, K., Flögel, S., Liebetrau, V., Posenato, R., Angiolini, L., Garbelli, C., Brand, U., Wiedenbeck, M. & Eisenhauer, A. (2020) Permian-Triassic mass extinction pulses driven by major marine carbon cycle perturbations. *Nature Geoscience*, 13, 745–750. https://doi.org/10.1038/s41561-020-00646-4

Korte, C., Jasper, T., Kozur, H.W. & Veizer, J. (2006) 87Sr/86Sr record of Permian seawater. *Palaeogeography, Palaeoclimatology, Palaeoecology*, 240 (1-2), 89–107. https://doi.org/10.1016/j.palaeo.2006.03.047

Korte, C., Kozur, H.W., Bruckschen, P. & Veizer, J. (2003) Strontium isotope evolution of Late Permian and Triassic seawater. *Geochimica et Cosmochimica Acta*, 67 (1), 47–62. https://doi.org/10.1016/S0016-7037(02)01035-9

Lau, K.V., Maher, K., Altiner, D., Kelley, B.M., Kump, L.R., Lehrmann, D.J., Silva-Tamayo, J.C., Weaver, K.L., Yu, M.Y.

& Payne, J.L. (2016) Marine anoxia and delayed Earth system recovery after the end-Permian extinction. *Proceedings of the National Academy of Sciences of the United States of America*, 113 (9), 2360–2365.
https://doi.org/10.1073/pnas.1515080113

Lemarchand, E., Chabaux, F., Vigier, N., Millot, R. & Pierret, M.C. (2010) Lithium isotope systematics in a forested granitic catchment (Strengbach, Vosges Mountains, France). *Geochimica et Cosmochimica Acta*, 74 (16), 4612–4628.
https://doi.org/10.1016/j.gca.2010.04.057

Li, G. & West, A.J. (2014) Evolution of Cenozoic seawater lithium isotopes: Coupling of global denudation regime and shifting seawater sinks. *Earth and Planetary Science Letters*, 401, 284–293.
https://doi.org/10.1016/j.epsl.2014.06.011

Liao, Z.W., Hu, W.X., Cao, J., Wang, X.L., Yao, S.P., Wu, H.G. & Wan, Y. (2016) Heterogeneous volcanism across the Permian-Triassic Boundary in South China and implications for the Latest Permian Mass Extinction: New evidence from volcanic ash layers in the Lower Yangtze Region. *Journal of Asian Earth Sciences*, 127, 197–210.
https://doi.org/10.1016/j.jseaes.2016.06.003

Ling, M.X., Sedaghatpour, F., Teng, F.Z., Hays, P.D., Strauss, J. & Sun, W.D. (2011) Homogeneous magnesium isotopic composition of seawater: an excellent geostandard for Mg isotope analysis. *Rapid Communications in Mass Spectrometry*, 25 (19), 2828–2836.
https://doi.org/10.1002/rcm.5172

Liu, C., Jiang, T.E., Yang, Y. & Ma, J. (2023) Temporal and spatial variations of high-resolution strontium, carbon, and oxygen isotopic chemostratigraphy at the end-Permian crisis boundary in South China. *Gondwana Research*, 113, 89–101.
https://doi.org/10.1016/j.gr.2022.10.015

Liu, X.Y., Krause, A.J., Wilson, D.J., Fraser, W.T., Joachimski, M.M., Brand, U., Stigall, A.L., Qie, W.K., Chen, B., Yang, X.R. & Pogge von Strandmann, P.A.E. (2025) Lithium isotope evidence shows Devonian afforestation may have significantly altered the global silicate weathering regime. *Geochimica et Cosmochimica Acta*, 396, 107–121.
https://doi.org/10.1016/j.gca.2025.02.036

Liu, Z.Y. & Selby, D. (2021) Deep-water osmium-isotope record of the Permian-Triassic interval from Niushan, China reveals potential delayed volcanic signal post the mass extinction. *Global and Planetary Change*, 200, 103473.
https://doi.org/10.1016/j.gloplacha.2021.103473

Liu, Z.Y., Selby, D., Zhang, H. & Shen, S.Z. (2020) Evidence for volcanism and weathering during the Permian-Triassic mass extinction from Meishan (South China) osmium isotope record. *Palaeogeography, Palaeoclimatology, Palaeoecology*, 553, 109790.
https://doi.org/10.1016/j.palaeo.2020.109790

Mackenzie, F.T. & Kump, L.R. (1995) Reverse Weathering, Clay Mineral Formation, and Oceanic Element Cycles. *Science*, 270 (5236), 586.
https://doi.org/10.1126/science.270.5236.586

McLennan, S.M. & Taylor, S.R. (1991) Sedimentary Rocks and Crustal Evolution: Tectonic Setting and Secular Trends. *Journal of Geology*, 99 (1), 1–21.
https://doi.org/10.1086/629470

Misra, S. & Froelich, P.N. (2012) Lithium Isotope History of Cenozoic Seawater: Changes in Silicate Weathering and Reverse Weathering. *Science*, 335 (6070), 818–823.
https://doi.org/10.1126/science.1214697

Nesbitt, H.W. & Young, G.M. (1982) Early Proterozoic climates and plate motions inferred from major element chemistry of lutites. *Nature*, 299 (5885), 715–717.
https://doi.org/10.1038/299715a0

Nsingi, J.M., Cui, Y., Cepin, E., Beaty, B., Planavsky, N., Wu, Q., Adloff, M., Wang, J., Selby, D., Liu, Z., Dong, Y., Jiang, S. & Zhu, F. (2025) Changes in continental weathering across the Permian-Triassic transition: A global review. *Global and Planetary Change*, 254, 105015.
https://doi.org/10.1016/j.gloplacha.2025.105015

Palmer, M.R. & Edmond, J.M. (1989) The Strontium Isotope Budget of the Modern Ocean. *Earth and Planetary Science Letters*, 92 (1), 11–26.
https://doi.org/10.1016/0012-821X(89)90017-4

Pearce, C.R., Parkinson, I.J., Gaillardet, J., Charlier, B.L.A., Mokadem, F. & Burton, K.W. (2015) Reassessing the stable (δ^{88}/86Sr) and radiogenic (87Sr/86Sr) strontium isotopic composition of marine inputs. *Geochimica et Cosmochimica Acta*, 157, 125–146.
https://doi.org/10.1016/j.gca.2015.02.029

Peucker-Ehrenbrink, B. & Fiske, G.J. (2019) A continental perspective of the seawater 87Sr/86Sr record: A review. *Chemical Geology*, 510, 140–165.
https://doi.org/10.1016/j.chemgeo.2019.01.017

Peucker-Ehrenbrink, B. & Ravizza, G. (2000) The marine osmium isotope record. *Terra Nova*, 12 (5), 205–219.
https://doi.org/10.1046/j.1365-3121.2000.00295.x

Pogge von Strandmann, P.A.E., Burton, K.W., James, R.H., van Calsteren, P., Gislason, S.R. & Sigfússon, B. (2008) The influence of weathering processes on riverine magnesium isotopes in a basaltic terrain. *Earth and Planetary Science Letters*, 276 (1-2), 187–197.
https://doi.org/10.1016/j.epsl.2008.09.020

Pogge von Strandmann, P.A.E., Jenkyns, H.C. & Woodfine, R.G. (2013) Lithium isotope evidence for enhanced weathering during Oceanic Anoxic Event 2. *Nature Geoscience*, 6, 668–672.
https://doi.org/10.1038/ngeo1875

Pogge von Strandmann, P.A.E., Schmidt, D.N., Planavsky, N.J., Wei, G., Jones, C.L. & Baumann, K.H. (2019) Assessing bulk carbonates as archives for seawater Li isotope ratios. *Chemical Geology*, 530, 119338.
https://doi.org/10.1016/j.chemgeo.2019.119338

Pogge von Strandmann, P.A.E., Dellinger, M. & West, A.J.

(2021) Lithium isotopes: a tracer of past and present silicate weathering. *Geochemical Tracers in Earth System Science*. https://doi.org/10.1017/9781108990752

Pogge von Strandmann, P.A.E., Liu, X.Y., Liu, C.Y., Wilson, D.J., Hammond, S.J., Tarbuck, G., Aristilde, L., Krause, A.J. & Fraser, W.T. (2022) Lithium isotope behaviour during basalt weathering experiments amended with organic acids. *Geochimica et Cosmochimica Acta*, 328, 37–57. https://doi.org/10.1016/j.gca.2022.04.032

Pogge von Strandmann, P.A.E., Cosford, L.R., Liu, C.Y., Liu, X.Y., Krause, A.J., Wilson, D.J., He, X.Q., McCoy-West, A.J., Gislason, S.R. & Burton, K.W. (2023) Assessing hydrological controls on the lithium isotope weathering tracer. *Chemical Geology*, 642, 121801. https://doi.org/10.1016/j.chemgeo.2023.121801

Qie, W.K., Zhang, J.P., Luo, G.M., Algeo, T.J., Chen, B., Xiang, L., Liang, K., Liu, X.Y., Pogge von Strandmann, P.A.E., Chen, J.T. & Wang, X.D. (2023) Enhanced Continental Weathering as a Trigger for the End-Devonian Hangenberg Crisis. *Geophysical Research Letters*, 50 (11), e2022GL102640. https://doi.org/10.1029/2022GL102640

Rauzi, S., Foster, W.J., Takahashi, S., Hori, R.S., Beaty, B.J., Tarhan, L.G. & Isson, T. (2024) Lithium isotopic evidence for enhanced reverse weathering during the Early Triassic warm period. *Proceedings of the National Academy of Sciences of the United States of America*, 121 (32), e2318860121. https://doi.org/10.1073/pnas.2318860121

Rooney, A.D., Selby, D., Lloyd, J.M., Roberts, D.H., Lückge, A., Sageman, B.B. & Prouty, N.G. (2016) Tracking millennial-scale Holocene glacial advance and retreat using osmium isotopes: Insights from the Greenland ice sheet. *Quaternary Science Reviews*, 138, 49–61. https://doi.org/10.1016/j.quascirev.2016.02.021

Schneebeli-Hermann, E., Kurschner, W.M., Hochuli, P.A., Ware, D., Weissert, H., Bernasconi, S.M., Roohi, G., ur-Rehman, K., Goudemand, N. & Bucher, H. (2013) Evidence for atmospheric carbon injection during the end-Permian extinction. *Geology*, 41 (5), 579–582. https://doi.org/10.1130/G34047.1

Schoepfer, S.D., Henderson, C.M., Garrison, G.H., Foriel, J., Ward, P.D., Selby, D., Hower, J.C., Algeo, T.J. & Shen, Y.N. (2013) Termination of a continent-margin upwelling system at the Permian-Triassic boundary (Opal Creek, Alberta, Canada). *Global and Planetary Change*, 105, 21–35. https://doi.org/10.1016/j.gloplacha.2012.07.005

Sedlacek, A.R.C., Saltzman, M.R., Algeo, T.J., Horacek, M., Brandner, R., Foland, K. & Denniston, R.F. (2014) 87Sr/86Sr stratigraphy from the Early Triassic of Zal, Iran: Linking temperature to weathering rates and the tempo of ecosystem recovery. *Geology*, 42 (9), 779–782. https://doi.org/10.1130/G35545.1

Song, H.J., Wignall, P.B., Tong, J.N., Song, H.Y., Chen, J., Chu, D.L., Tian, L., Luo, M., Zong, K.Q., Chen, Y.L., Lai, X.L., Zhang, K.X. & Wang, H.M. (2015) Integrated Sr isotope variations and global environmental changes through the Late Permian to early Late Triassic. *Earth and Planetary Science Letters*, 424, 140–147. https://doi.org/10.1016/j.epsl.2015.05.035

Spalletti, L.A. & Limarino, C.O. (2017) The Choiyoi magmatism in south western Gondwana: implications for the end-permian mass extinction—a review. *Andean Geology*, 44 (3), 328–338. https://doi.org/10.5027/andgeoV44n3-a05

Sun, H., Xiao, Y., Gao, Y., Zhang, G., Casey, J.F. & Shen, Y. (2018) Rapid enhancement of chemical weathering recorded by extremely light seawater lithium isotopes at the Permian-Triassic boundary. *Proceedings of the National Academy of Sciences of the United States of America*, 115 (15), 3782–3787. https://doi.org/10.1073/pnas.1711862115

Sun, Y.D., Joachimski, M.M., Wignall, P.B., Yan, C.B., Chen, Y.L., Jiang, H.S., Wang, L.N. & Lai, X.L. (2012) Lethally Hot Temperatures During the Early Triassic Greenhouse. *Science*, 338 (6105), 366–370. https://doi.org/10.1126/science.1224126

Svensen, H., Planke, S., Polozov, A.G., Schmidbauer, N., Corfu, F., Podladchikov, Y.Y. & Jamtveit, B. (2009) Siberian gas venting and the end-Permian environmental crisis. *Earth and Planetary Science Letters*, 277 (3-4), 490–500. https://doi.org/10.1016/j.epsl.2008.11.015

Taylor, K., Rauzi, S., Isson, T., Ibarra, D.E., Hülse, D., Kimmig, S.R., Payne, J.L., Altiner, D., Lehrmann, D.J., Kalderon-Asael, B., Planavsky, N.J. & Lau, K.V. (2026) Heterogeneous Carbonate Lithium Isotope Records Across the end-Permian Mass Extinction Indicate a Highly Perturbed Lithium Cycle in the Early Triassic. *American Journal of Science*, 326, Article 5. https://doi.org/10.2475/001c.156171

Tipper, E.T., Galy, A. & Bickle, M.J. (2006) Riverine evidence for a fractionated reservoir of Ca and Mg on the continents: Implications for the oceanic Ca cycle. *Earth and Planetary Science Letters*, 247 (3-4), 267–279. https://doi.org/10.1016/j.epsl.2006.04.033

Tomascak, P.B. (2004) Developments in the understanding and application of lithium isotopes in the earth and planetary sciences. *Reviews in Mineralogy and Geochemistry*, 55 (1), 153–195. https://doi.org/10.2138/gsrmg.55.1.153

Veevers, J.J. & Tewari, R.C. (1995) Permian-Carboniferous and Permian-Triassic magmatism in the rift-zone bordering the Tethyan margin of southern Pangea. *Geology*, 23 (5), 467–470. https://doi.org/10.1130/0091-7613(1995)023<0467:PCAPTM>2.3.CO;2

Veizer, J., Ala, D., Azmy, K., Bruckschen, P., Buhl, D., Bruhn, F., Carden, G.A.F., Diener, A., Ebneth, S., Godderis, Y., Jasper, T., Korte, C., Pawellek, F., Podlaha, O.G. & Strauss, H. (1999) 87Sr/86Sr, $\delta^{13}C$ and $\delta^{18}O$ evolution of Phanerozoic seawater. *Chemical Geology*, 161 (1-3), 59–88. https://doi.org/10.1016/S0009-2541(99)00081-9

Vigier, N., Decarreau, A., Millot, R., Carignan, J., Petit, S. & France-Lanord, C. (2008) Quantifying Li isotope fractionation during smectite formation and implications for the Li cycle. *Geochimica et Cosmochimica Acta*, 72 (3), 780–792. https://doi.org/10.1016/j.gca.2007.11.011

Viglietti, P.A., Benson, R.B.J., Smith, R.M.H., Botha, J., Kammerer, C.F., Skosan, Z., Butler, E., Crean, A., Eloff, B., Kaal, S., Mohoi, J., Molehe, W., Mtalana, N., Mtungata, S., Ntheri, N., Ntsala, T., Nyaphuli, J., October, P., Skinner, G., Strong, M., Stummer, H., Wolvaardt, F.P. & Angielczyk, K.D. (2021) Evidence from South Africa for a protracted end-Permian extinction on land. *Proceedings of the National Academy of Sciences of the United States of America*, 118 (17), e2017045118. https://doi.org/10.1073/pnas.2017045118

Walker, J.C.G., Hays, P.B. & Kasting, J.F. (1981) A negative feedback mechanism for the long-term stabilization of Earth's surface temperature. *Journal of Geophysical Research*, 86 (C10), 9776–9782. https://doi.org/10.1029/JC086iC10p09776

Wang, J.Y., Jacobson, A.D., Zhang, H., Ramezani, J., Sageman, B.B., Hurtgen, M.T., Bowring, S.A. & Shen, S.Z. (2019) Coupled δ44/40Ca, δ88/86Sr, and 87Sr/86Sr geochemistry across the end-Permian mass extinction event. *Geochimica et Cosmochimica Acta*, 262, 143–165. https://doi.org/10.1016/j.gca.2019.07.035

Wang, W.Q., Katchinoff, J.A.R., Garbelli, C., Immenhauser, A., Zheng, Q.F., Zhang, Y.C., Yuan, D.X., Shi, Y.K., Wang, J.Y., Planavsky, N. & Shen, S.Z. (2021) Revisiting the Permian seawater 87Sr/86Sr record: New perspectives from brachiopod proxy data and stochastic oceanic box models. *Earth-Science Reviews*, 218, 103679. https://doi.org/10.1016/j.earscirev.2021.103679

Wang, W.Q., Zhang, F.F., Liu, C.Y., Pogge von Strandmann, P.A.E., Xiong, G.L., Zheng, Q.F., Garbelli, C., Zhang, Y.C., Yuan, D.X. & Shen, S.Z. (2024) Constraints on the continental weathering intensity through the Permian using lithium isotopes of well-preserved brachiopod shells. *Earth and Planetary Science Letters*, 648, 119101. https://doi.org/10.1016/j.epsl.2024.119101

Washington, K.E., West, A.J., Kalderon-Asael, B., Katchinoff, J.A.R., Stevenson, E.I. & Planavsky, N.J. (2020) Lithium isotope composition of modern and fossilized Cenozoic brachiopods. *Geology*, 48 (11), 1058–1061. https://doi.org/10.1130/G47558.1

Wei, G.Y., Wei, W., Wang, D., Li, T., Yang, X., Shields, G.A., Zhang, F., Li, G., Chen, T., Yang, T. & Ling, H.F. (2020) Enhanced chemical weathering triggered an expansion of euxinic seawater in the aftermath of the Sturtian glaciation. *Earth and Planetary Science Letters*, 539, 116244. https://doi.org/10.1016/j.epsl.2020.116244

Wei, G.Y., Zhao, M.Y., Sperling, E.A., Gaines, R.R., Kalderon-Asael, B., Shen, J., Li, C., Zhang, F.F., Li, G.J., Zhou, C.M., Cai, C.F., Chen, D.Z., Xiao, K.Q., Jiang, L., Ling, H.F., Planavsky, N.J. & Tarhan, L.G. (2024) Lithium isotopic constraints on the evolution of continental clay mineral factory and marine oxygenation in the earliest Paleozoic Era. *Science Advances*, 10 (13), eadk2152. https://doi.org/10.1126/sciadv.adk2152

Wimpenny, J., Colla, C.A., Yin, Q.Z., Rustad, J.R. & Casey, W.H. (2014) Investigating the behaviour of Mg isotopes during the formation of clay minerals. *Geochimica et Cosmochimica Acta*, 128, 178–194. https://doi.org/10.1016/j.gca.2013.12.012

Wimpenny, J., Gíslason, S.R., James, R.H., Gannoun, A., Pogge von Strandmann, P.A.E. & Burton, K.W. (2010) The behaviour of Li and Mg isotopes during primary phase dissolution and secondary mineral formation in basalt. *Geochimica et Cosmochimica Acta*, 74 (18), 5259–5279. https://doi.org/10.1016/j.gca.2010.06.028

Wu, Q., Ramezani, J., Zhang, H., Wang, J., Zeng, F., Zhang, Y., Liu, F., Chen, J., Cai, Y., Hou, Z., Liu, C., Yang, W., Henderson, C.M. & Shen, S.Z. (2021) High-precision U-Pb age constraints on the Permian floral turnovers, paleoclimate change, and tectonics of the North China block. *Geology*, 49 (6), 677–681. https://doi.org/10.1130/G48051.1

Xu, G.Z., Shen, J., Algeo, T.J., Yu, J.X., Feng, Q.L., Frank, T.D., Fielding, C.R., Yan, J.X., Deconink, J.F. & Lei, Y. (2023) Limited change in silicate chemical weathering intensity during the Permian-Triassic transition indicates ineffective climate regulation by weathering feedbacks. *Earth and Planetary Science Letters*, 616, 118235. https://doi.org/10.1016/j.epsl.2023.118235

Ye, R.H., Zhang, F.F., Wei, G.Y., Chen, J.B., Feng, Z. & Shen, S.Z. (2024) Lithium isotopes track changes in continental weathering regimes across the end-Permian mass extinction in Southwest China. *Earth and Planetary Science Letters*, 647, 119045. https://doi.org/10.1016/j.epsl.2024.119045

Zhang, H.R., Yang, T.N., Hou, Z.Q., Song, Y.C., Ding, Y. & Cheng, X.F. (2013) Petrogenesis and tectonics of late Permian felsic volcanic rocks, eastern Qiangtang block, north-central Tibet: Sr and Nd isotopic evidence. *International Geology Review*, 55 (8), 1017–1028. https://doi.org/10.1080/00206814.2012.759669

Zhang, H., Zhang, F.F., Chen, J.B., Erwin, D.H., Syverson, D.D., Ni, P., Rampino, M., Chi, Z., Cai, Y.F., Xiang, L., Li, W.Q., Liu, S.A., Wang, R.C., Wang, X.D., Feng, Z., Li, H.M., Zhang, T., Cai, H.M., Zheng, W., Cui, Y., Zhu, X.K., Hou, Z.Q., Wu, F.Y., Xu, Y.G., Planavsky, N. & Shen, S.Z. (2021) Felsic volcanism as a factor driving the end-Permian mass extinction. *Science Advances*, 7 (47), eabh1390. https://doi.org/10.1126/sciadv.abh1390

Zhang, P.X., Yang, M.F, Lu, J., Bond, D.P., Zhou, K., Xu, X.T., Wang, Y., He, Z., Bian, X., Shao, L.Y. & Hilton, J. (2023) End-Permian terrestrial ecosystem collapse in North China: evidence from palynology and geochemistry. *Global and*

Planetary Change, 222, 104070.
https://doi.org/10.1016/j.gloplacha.2023.104070

Zhao, H., Zhang, L., Algeo, T.J., Lyu, Z., Wang, X. & Hao, F. (2025) Volcanism and basalt weathering drove Ordovician climatic cooling. *Nature Communications*, 16, 11475.
https://doi.org/10.1038/s41467-025-66316-4

Zhou, J.L., Zhang, F.F., Lin, Y.B., Ren, G.Y., Wei, G.Y., Yang, A.H. & Shen, S.Z. (2025) Paired lithium and barium isotopes uncover weathering and productivity controls on the late cambrian SPICE event. *Geochimica et Cosmochimica Acta*, 410, 188–202.
https://doi.org/10.1016/j.gca.2025.10.011